Enhanced Electrochemical Stability by Alkyldiammonium in Dion-Jacobson Perovskite Towards Ultrastable Light-Emitting Diodes

Kwanho Ngai
The Chinese University of Hong Kong
Qi Wei
University of Macau https://orcid.org/0000-0002-5322-3692
Zefeng Chen
Chinese University of Hong Kong
Xinlu Guo
Chinese University of Hong Kong
Minchao Qin
The Chinese University of Hong Kong https://orcid.org/0000-0001-8819-2307
Christopher C. S. Chan
Hong Kong University of Science and Technology https://orcid.org/0000-0001-6725-6463
Guichuan Xing
University of Macau https://orcid.org/0000-0003-2769-8659
Xinhui Lu
Chinese University of Hong Kong
Fangyan Xie
Sun Yat-sen University
Jian Chen
Sun Yat-sen University
Jian-Bin Xu
The Chinese University of Hong Kong https://orcid.org/0000-0003-0509-9508
Kam Sing Wong
The Hong Kong University of Science and Technology
Mingzhu Long (mzlong@ee.cuhk.edu.hk)
The Chinese University of Hong Kong

Article

Keywords: Alkyldiammonium, perovskite light-emitting diodes (PeLEDs), Dion-Jacobson Perovskite

Posted Date: December 1st, 2020

DOI: https://doi.org/10.21203/rs.3.rs-114159/v1

Abstract

The electroluminescence efficiency of perovskite light-emitting diodes (PeLEDs) has gained notable achievements, but the poor stability under electric stress severely impedes future practical use. Here, an alkyldiammonium 1,4-butanediamine (BDA) is incorporated into perovskite emitting layer, which substantially optimizes electrochemical stability and minimizes interfacial deep traps under large external bias. The BDA-PeLED shows a record operational half-lifetime T_{50} of 189.4 h at a high current density of 100 mA cm^{-2} and 589 hours under 50 mA cm^{-2}. Additionally, the device maintains its original performance upon 2500 cycles of voltage scan and withstands 10000 times of ON-OFF under a pulsed voltage of 2.5 V. Further degradation mechanism study reveals that the main origins of the instability property of PeLEDs without BDA are the generation of deep traps at the interfaces and the infiltration of anions into adjacent layers. The significantly enhanced electrochemical stability suggests that alkyldiammonium cation incorporation provides a direction to solve the instability issue.

Introduction

Metal halide perovskite materials have been gaining unprecedented improvements in the field of light-emitting diodes (LEDs) due to the distinctive merits of tunable emission color ranging from ultraviolet to near-infrared wavelength, high color purity, high photoluminescence quantum efficiency (PLQE) and balanced carrier mobility[1-8]. Additionally, the facile solution processable feature of perovskite emitting layers make the devices compatible with roll-to-roll fabrication process, demonstrating a promising application in flexible and wearable electronics[9, 10]. Over the past several years, the external quantum efficiency (EQE) value of perovskite light-emitting diodes (PeLEDs) has exceeded over 20% through continuous research efforts on perovskite composition tuning, defect passivation, charge injection balancing and light extraction enhancement[4, 5, 11, 12].

Despite the achievement of excellent electroluminescence (EL) performance, PeLEDs with operational half-lifetime (T_{50}) less than several hours under inert atmosphere have been widely reported. The short operational lifetime severely hampers the commercialization process of PeLEDs. In response to the instability issue under electric field, various strategies have been developed to improve the lifetime, while the T_{50} exceeding one hundred hours is rarely reported, lagging far behind that of perovskite solar cells, which can be closely related to the higher working bias required for PeLEDs. Degradation mechanism studies demonstrate that ion migration in perovskite structure, Joule heating and instability of injection layers under electric field are the main causes of the poor stability[13-16]. The severe ion drift in perovskite upon electric field during operation results in the emission wavelength shift[17], the decomposition of perovskite layer[18], the interfacial reaction between perovskite and injection materials/electrode layers[14, 19], giving rise to a completely irreversible degradation after prolonged operation.

The strategy of defect passivation through various passivation agents (PA) has been employed to annihilate defects at grain boundaries and on film surface, thus reducing the nonradiative recombination

and suppressing the defect-assisted ion migration process in perovskite structure. The suppressed ion migration can not only significantly improve EQE value and optimize the spectral stability at large bias voltage, but also improve operational lifetime[20]. Moreover, different monovalent organic cations in perovskite structure have been demonstrated to have a strong impact on the stability of PeLEDs. For formamidinium (FA)-based perovskite, it possesses a much higher atomic density compared to that of methylammonium (MA)-based perovskite, so the mobile ion migration can be greatly mitigated due to larger formation energy of defects and stronger hydrogen bonding between organic cation and inorganic framework[21, 22]. Inorganic cations Cs^+ and Rb^+ have been employed to decrease the defect density and increase the ion migration barrier, achieving a significant stability improvement in PeLEDs[12, 23]. Additionally, bulky organic cations have been incorporated into perovskite precursor to form quasi-2D Ruddlesden-Popper (RP) structure, in which the insulating organic layer is a natural barrier for ion migration, leading to a stable emission peak and prolonged lifetime[24-27]. It was demonstrated that the surface treatment on 3D perovskite by an aromatic cation benzylammonium could result in an improved T_{50} of 23.7 h under a current density of 100 mA cm^{-2}. [28] Recently, a divalent cation 1,4-bis(aminomethyl)benzene with large molecular size has been employed as bridging ligand in a layered perovskite to form a Dion-Jacobson (DJ) structure and applied in PeLEDs for the first time, which demonstrated a low efficiency roll-off at high current density and two-orders of magnitude longer T_{50} lifetime than that of RP-based PeLEDs[29]. The surprisingly elongated lifetime can be attributed to the enhanced bonding energy between the organic cation and inorganic layers. Nevertheless, despite the promising lifetime of PeLEDs based on DJ structure, the achieved peak EQE is much lower than that of three-dimensional perovskite-based LEDs (3D-PeLEDs). Besides, the mechanism for lifetime enhancement for PeLEDs based on DJ perovskite should be further investigated and comprehensively understood.

In this work, an alkyldiammonium cation 1,4-butanediamine (BDA) with a moderate molecular size is incorporated into 3D perovskite, leading to the formation of a typical layered DJ perovskite structure, which can effectively optimize the EL performances and suppress the interfacial electrochemical reaction, as well as mitigate the ion interfusion into adjacent layers in PeLEDs under large electric field. Through judiciously tuning the phase composition of the DJ perovskite, the BDA-PeLED shows an operational half-lifetime T_{50} of 189.4 h at a high injection current of 100 mA cm^{-2}, while the T_{50} of 3D-PeLEDs is only 10 h. The T_{50} of the BDA-PeLED is prolonged to 589 h under an operational current of 50 mA cm^{-2}. To the best of our knowledge, this is so far the longest lifetime reported for PeLEDs operated at this large current density. Moreover, the device maintains its initial performance upon 2500 cycles of voltage scan and withstands 10000 times of ON and OFF upon a 2.5 V and 2.5 Hz pulsed voltage. Degradation mechanism study demonstrates that the main causes of the poor stability for 3D-PeLEDs are the generation of high concentration of interfacial deep traps and severe infiltration of halide anions into adjacent injection layers. Additionally, the EQE of 1.8FA BDA-PeLEDs reaches to 16.4% after optimizing the crystal orientation and charge transport nature. The extraordinary performances of BDA-

PeLEDs suggest that the introduction of alkyldiammonium cations have great potential to further optimize electroluminescent efficiency and operational lifetime of PeLEDs.

Results

Properties of $BDAFA_{n-1}Pb_nI_{3n+1}$ thin films. $BDAFA_{n-1}Pb_nI_{3n+1}$ perovskite thin films with different *n* values (*n*=1-6) were deposited onto the ITO/ZnO/PEIE substrates through a typical one-step spin-coating process. Perovskite precursors are comprised of stoichiometric amounts of reactants, namely $BDAI_2$, PbI_2 and FAI, in the corresponding formula $BDAFA_{n-1}Pb_nI_{3n+1}$. The typical layered structures are schematically shown in Fig. 1A, with alkyldiammonium cation BDA^{2+} acting as bridging ligand between $[PbI_6]^{4-}$ octahedral layers. The X-ray diffraction (XRD) patterns of the quasi-2D DJ structure with different *n* values are presented in Fig. 1B. For *n*=1 $BDAPbI_4$ thin film, strong diffraction peaks at 8.6° and 14.6° are observed, which correspond to (001) and (1 1) planes, respectively[30, 31]. For *n*=2, 3 and 4 thin films, new diffraction peaks at 8.5°, 10.3° and 10.9° in small-angle diffraction range appear. The aperiodic and low-intensity diffraction peaks reflect a mixture of DJ phases with different n values in the quasi-2D film and a random crystallographic orientation of the crystalline structure. Another diffraction peak at 14.1° is presented in *n*=2-6 thin films, which can stem from the formation of DJ phase with large-*n* value (*n*=∞) during annealing process. Grazing incidence wide-angle X-ray scattering (GIWAXS) results further confirm a random crystallinity and the decreased orientation with the increase of *n* in the DJ film as shown in Supplementary Fig. 1. For the n=5 and 6 samples, the strong diffraction peak at 11.7° can be attributed to the formation of *δ*-$FAPbI_3$ phase and becomes disappeared after annealing at high temperature as shown in Supplementary Fig. 2.

Steady-state absorption spectra of the DJ perovskite series are displayed in Fig. 1C, of which the optical absorption edges are relatively sharp and the energy decreases with the increase of *n* value. The excitonic peaks can be obviously seen for the n=1-4 thin films which are the typical features of the layered perovskite. The *n*=1 phase shows a strong excitonic absorption peak at 493 nm, featuring an optical bandgap E_g of 2.52 eV. With the increase of *n* value, the absorption peak changes from 582 nm, 632 nm to 678 nm for *n*=2, 3 and 4 series, respectively. An analogous trend can be observed in the steady-state photoluminescence (PL) spectra in Fig. 1D. The PL peaks gradually shift from 511, 657, 681 to 688 nm for *n*=1, 2, 3 and 4 DJ films, respectively. For the n=5 and 6 DJ thin films, the excitonic absorption peak becomes indistinct in the steady-state absorbance curves and PL peak position is very close to that of 3D $FAPbI_3$ perovskite, which can be attributed to the strong interlayer coupling and weak quantum confinement in the large-n DJ phases[32]. Furthermore, owing to the excellent thermal stability of DJ perovskite, a higher annealing temperature is applied to optimize the crystallinity and tune the 2D/3D phase composition with PL spectra shown in Fig. 1D. The peak position shows a large red shift and the intensity becomes much stronger with the increase of annealing temperature. For *n*=2-6 thin films, PL peak position difference is very small and close to that of 3D $FAPbI_3$ film as shown in Supplementary Fig. 3, illustrating that large-*n* (*n*=∞) phase tends to be formed and the composition of small-*n* DJ phases is decreased. The XRD pattern comparison in Supplementary Fig. 2 together with the PL behavior manifests

that a higher annealing temperature can significantly optimize both the crystal orientation and radiative recombination in DJ thin films, which has great advantages for light emitting applications. Furthermore, to confirm the phase transition for the DJ thin film after annealing at higher temperature, transient absorption (TA) spectroscopy is employed to investigate the phase composition in the n=5 thin film as shown in Fig. 1E. The n=5 BDA-DJ film is chosen due to its PL position close to that of 3D-$FAPbI_3$ and the PL positions for the thin films after annealing at 100 and 140 °C are quite different. There are obvious bleaching peaks observed at 578 nm, 635 nm and 674 nm for the thin film after annealing at 100 °C, which are consistent with the steady-state absorption results. Besides, the rising of the photobleaching peak at 745 nm is obviously observed for the sample with high annealing temperature, suggesting the formation of large-n phase and red-shift of the PL peak position.

Electroluminescent performance of BDA-PeLEDs. PeLEDs based on BDA-DJ perovskite films with different-*n* (*n*=2-6) values were fabricated through solution process with a device structure of ITO/ZnO/PEIE/$BDAFA_{n-1}Pb_nI_{3n+1}$/TFB/MoO_3/Au as illustrated in Supplementary Fig. 4. For simplicity, BDA-PeLEDs and 3D-PeLEDs are used to represent PeLEDs with or without BDA incorporation. The electroluminescent performances of the BDA-PeLEDs with different *n* values are displayed in Fig. 2A and 2B. The maximum EQE and radiance increase obviously with the increase of *n* value in the DJ phases, with EQE values ranging from 1.4%, 2.6%, 4.0%, 4.4% to 4.7% and radiance intensities from 29.8, 48.1, 95.8, 131.4 to 148.9 W Sr^{-1} m^{-2} for *n*=2-6 BDA-PeLED samples, respectively. All the BDA-PeLEDs with different *n* values demonstrate a high current density and a low turn-on voltage of approximate 1.4 V as shown in Supplementary Fig. 5, illustrating a low resistance and high carrier mobility of the $BDAFA_{n-1}Pb_nI_{3n+1}$ DJ thin films despite the nonuniform morphology shown in Supplementary Fig. 6. As mentioned in Supplementary Fig. 2, although a higher annealing temperature facilitates the formation of large-*n* phase and optimizes the crystallinity, PbI_2 and *δ*-$FAPbI_3$ impurities are apparently formed in the thin film. To suppress the impurity phases and optimize the radiative recombination in the emitting layer, excess FAI has been incorporated in the thin film[33]. As the *n*=5 and 6 BDA-PeLEDs show a little variance on electroluminescent performances, the *n*=5 sample is chosen to further evaluate the effect of excess FAI composition on the EL performances with FAI to PbI_2 ratio increasing from 1.7 to 2.3. For simplicity, the FAI to PbI_2 ratio is used to represent the device with different FAI ratios, for instance, PeLED based on DJ perovskite with FAI to PbI_2 ratio of 1.8 was named as 1.8FA BDA-PeLED.

The EQE and radiance intensity as a function of current density are demonstrated in Fig. 2C and 2D, respectively. EQE value increases obviously with the increase of FA amount in the *n*=5 DJ film from 6.7% for 1.7FA to 10.3% for 2.2FA, and decreases slightly to 10.1% for 2.3FA BDA-PeLEDs. The radiance intensity increases simultaneously from 183.9 W Sr^{-1} m^{-2} for 1.7FA to the highest value of 482.4 W Sr^{-1} m^{-2} for 1.9FA and then decreases with further increase of FA content. Notably, the 1.8FA BDA-PeLED can maintain over 90% of its peak EQE value at a high current density of 1000 mA cm^{-2} as displayed in Fig. 2C, which implies a reliable operational stability under large electric field. The EQE roll-off becomes larger with FA to Pb ratio exceeding 1.8 as indicated in Fig. 2C, which could be attributed to the efficiency

quenching by non-radiative Auger recombination under high injection current density[34]. Transmission scanning electron microscope (TEM) characterizations are conducted to check the phase composition of the 1.8FA n=5 DJ thin film as shown in Supplementary Fig. 7, which provide direct evidences for the presence of DJ phases at nanometer-length scale.

To further optimize the light emission efficiency, passivation agent (PA) 2,2'-[oxybis(ethylenoxy)]diethylamine has been incorporated into DJ thin film [6] and the performance is demonstrated in Fig. 2E and 2F. The 1.8FA BDA-PeLEDs with PA show an average value of 15.02% with the highest EQE reaching to 16.4% as indicated in Supplementary Fig. 8, while the radiance intensity decreases at large current density. The reduced radiance intensity and quick roll-off with additional amount of PA content, can tentatively render instability issue after long-term operation, despite the increase of EQE value and the suppression of trap centers. The XRD patterns and SEM images of the thin films with PA addition are provided in Supplementary Fig. 9, which demonstrate gradually increased crystallinity and decreased film coverage with the increase of PA amount. From the TA spectra of 1.8FA BDA-DJ thin films without/with PA as shown in Supplementary Fig. 10, there are narrow and intense bleaching peaks at 578 nm, 635 nm, 674 nm and 720 nm, which indicate the existence of n=2, 3, 4 and 5 BDA-DJ phases. From the normalized TA spectra of 1.8FA n=5 DJ thin film with the addition of PA, it can be observed that the bleaching peaks at 578 nm, 635 nm and 674 nm demonstrate ultrafast decay with the time constants of 0.26 ps, 0.35 ps and 0.36 ps, respectively. Besides, the rising time of bleaching peak at 765 nm is 0.46 ps which is consistent with the fast decay time of small-n DJ phases. The fast formation time of the photobleaching peak at long wavelength indicates the photo-generated excitons in small-n phases can be efficiently localized into large-n phase (n=∞). The ultrafast carrier localization and much longer carrier lifetime (Supplementary Fig. 10D), can contribute to the performance improvement after the addition of PA in the DJ thin film.

Operational lifetime of PeLEDs. As the 1.8FA BDA-PeLED possesses remarkably small EQE roll-off and reliable stability under current density over 1000 mA cm^{-2}, the operational lifetime is further evaluated under a large injection current of 100 mA cm^{-2} as shown in Fig. 3A. The device demonstrates 29% higher EQE than its initial value in the very beginning stage of the stability tracking and shows a T_{100} of 47.6 h (T_{100} is the time required for EQE falling to the initial value). The device can maintain 50% of its EQE value after continuous operation for 189.4 h (T_{50}). To the best of our knowledge, this is the longest lifetime reported for PeLEDs under a large current density of 100 mA cm^{-2} and the performance comparison of near-infrared PeLEDs is summarized in Supplementary Table 1. The voltage value during the operation is provided in Supplementary Fig. 11A which does not show obvious change during the whole decay process except for occasional fluctuation. The T_{50} of 1.8FA BDA-PeLED is further evaluated at 50 mA cm^{-2}, which is 589 h as shown in Supplementary Fig. 11B. To investigate the effect of BDA on the operational stability, 3D-PeLEDs based on $FAPbI_3$ with the same FA to Pb ratio of 1.8 were fabricated and the electroluminescent performance is shown in Supplementary Fig. 12. The EQE value drops to 50% of its initial value after continuous operation of 10 h under 100 mA cm^{-2} as shown in Fig. 3A, which is much shorter than that of 1.8FA BDA-PeLEDs. Moreover, the 1.8FA BDA-PeLEDs demonstrate excellent

stability upon 2500 cycles of forward voltage scan from 0 to 2.5 V as shown in Fig. 3B (scanning step of 0.1 V). The device can maintain 96% of its initial EQE value and the radiance does not show any appreciable decrease after the cycle scanning. The current density slightly increases after the 2500 cycles of scanning, suggesting very reliable stability of the BDA-DJ perovskite under electrical stress. An increase of EQE and radiance intensity is observed during the beginning of scanning cycles as indicated in Fig. 3C, which is probably attributed to trap healing by injected carriers in perovskite emitting layer[37]. However, for the 3D $FAPbI_3$ based device, both the EQE and radiance values demonstrate a large decrease after only 100 cycles of voltage scan shown in Fig. 3D and 3E. The current density falls by nearly a half, which results from the perovskite decomposition under electric field. Furthermore, the endurance of ON (light) and OFF (dark) switching for the 1.8FA BDA-PeLEDs is evaluated under a 2.5 Hz pulsed voltage of 2.5 V as illustrated in the inset of Fig. 3F. The EQE and radiance values during 10000 times of turn-on are summarized in Fig. 3F and Supplementary Fig. 13. The 1.8FA BDA-PeLED shows a small increase in both the EQE and radiance values at the beginning of the ON/OFF cycles, which is similar to the behavior observed under the voltage scan in Fig. 3C. The unabated performance indicates that the abrupt change of the voltage bias upon the device with such a large cycle does not deteriorate the optoelectronic properties of the BDA-DJ perovskite materials, further confirming a highly stable structure under electric field.

For the 3D-PeLEDs after degradation, there is an obvious degraded area on the Au electrode as shown in the inset of Fig. 3G and in Supplementary Fig. 14. PL spectra of the degraded and undegraded area demonstrate that the perovskite material beneath the degraded electrode area is completely decomposed and there does not exist any PL signal from perovskite phase. The boundary of the degraded area is partially decomposed, which indicates that the degradation of the 3D-PeLEDs under electric field is a spatially nonuniform process. The degradation of perovskite light emitting layer suggests that the intrinsic obstacle of operational lifetime for PeLEDs is the ion migration related electrochemical instability of perovskite emitting layer under electric stress. To understand ion migration behavior in perovskite under electric field, the activation energy of ion migration is evaluated through temperature-dependent voltage-current measurement with a lateral conduction configuration depicted in the inset of Fig. 3H and temperature ranging from 183 K to 383 K. The voltage-current curves under both forward and backward scans at different temperatures are summarized in Supplementary Fig. 15, which show a gradually increased current for both 3D- and BDA-DJ thin films with the increase of temperature. The transition temperature from electronic conductor to ionic conductor is 223 K for 3D $FAPbI_3$, which is lower than that for BDA-DJ perovskite material (273 K) and reflects mitigated ion migration in the structure with BDA incorporation. The activation energy was extracted from the ion conductor-dominant curve by the Nernst-Einstein relation as follows: , where is the Boltzmann constant and is a constant[38, 39]. The activation energy of mobile ion migration in 3D-$FAPbI_3$ perovskite material is estimated to be 0.21 eV, while the value of BDA-DJ perovskite is enlarged to 0.47 eV, fitted from the temperature-dependent conductivity as shown in Fig. 3H and 3I, respectively. The larger activation energy for BDA-DJ perovskite materials indicates the mitigated ion migration process in BDA-PeLEDs, which accounts for the lifetime improvement under long-term electric stress. The larger hysteresis of the voltage-current curves and the

deviation from the origin of the coordinates for 3D perovskite as shown in Supplementary Fig. 15 further suggest more severe ion migration issue. Besides, the EQE and radiance values of the BDA-PeLEDs obtained from reverse and forward voltage scans do not show any difference as shown in Supplementary Fig. 16, further confirming well suppressed ion migration in the light emitting layer and mitigated carrier accumulation at the interfaces of the devices.

Degradation behavior of PeLEDs. The degradation process of perovskite thin film under electric field is further *in-situ* observed under optical microscope. As demonstrated in Fig. 4A1-A3, the channel length between two electrodes in the lateral structure is 80 mm and the perovskite thin film was biased under an electric field of 35 V (0.44 V μm^{-1}). There is an obvious crack formed after being biased for 15 min as shown in Fig. 4A2, which is induced by migration of mobile ions under electric field. With the biasing time further increasing to 30 min, the crack shows a further movement towards the cathode electrode and becomes a bit wider, indicating more aggravated ion migration. PL characterization was conducted on the crack and its boundary areas as marked in Fig. 4A3. The PL intensity of the crack area (spot A) is very low compared to that of the undegraded area (spot D) as shown in Fig. 4B, suggesting a serious decomposition of the perovskite under electric field. The two-sides of the cracks (spot B and C) also shows remarkably decreased PL intensity, which may result from the opposite ion movement of organic cations and iodide anions driven by the electric field, namely, I^- moving towards anode and FA^+ moving towards cathode. On the contrary, the BDA-DJ perovskite thin film under electric stress does not show any appreciable degradation as shown in Supplementary Fig. 17.

To further investigate the effect of ion migration on the photoelectronic properties of different layers in PeLEDs, PL intensity and EQE of 3D-PeLEDs were monitored simultaneously during the degradation process as summarized in Fig. 4C. It demonstrates that EQE value of the device drops much faster than its PL intensity, which can be attributed to the deterioration of electronic properties of carrier injection layers or the interfaces. Furthermore, the optical images of Au electrode at different degradation stages including T_{100}, T_{50} and T_{20} in Fig. 4D1-D3 indicate that there is not any appreciable degradation in the vicinity of Au electrode before the degradation time of T_{50} as displayed in Fig. 4D2. Therefore, the degradation of EQE at the first stage can be largely derived from the destruction of electron/hole injection layer caused by electrochemical reaction. With degradation time further increased to T_{20}, the boundary area of the Au electrode exhibits an obvious morphology change and there are numerous black dots appeared on the surface as indicated in Fig. 4D3, which could be caused by ion infiltration from perovskite layer.

To investigate the vertical ion distribution in the device, X-ray photoelectronic spectroscopy (XPS) depth profile analysis was conducted for 3D- and BDA-PeLEDs after 20 h operation under 100 mA cm^{-2} as shown in Fig. 4E and 4F. The atomic ratio of iodide in Au electrode is a bit higher in 3D-PeLEDs than that in BDA-PeLEDs, which can be corresponding to the formation of black dots in Fig. 4D3 after severe degraded performance. The increased iodide ratio in TFB hole injection layer of 3D-PeLEDs suggests that the deterioration of the electronic properties caused by iodide migration is one of the main reasons for the

performance degradation. Besides, it is worth noting that the iodide ratio in the electron injection layer of ZnO is relatively high in both 3D- and BDA-PeLEDs, which can be attributed to the interfacial reaction between perovskite and ZnO. The high isoelectric point of the ZnO deprotonates the excess organic cations, resulting in the iodide ions drifting into the underneath carrier injection layer and Zn^{2+} drifting into the above perovskite layer[33]. The atomic ratio of iodide in the ZnO layer is much higher in 3D-PeLEDs than that in BDA-PeLEDs marked by dash line in Fig. 4E, which indicates more severe migration of iodide and electrochemical reaction across the interface under electric field.

The XPS spectra of iodide from different etching times in Fig. 4G directly confirm the existence of iodide in the Au electrode and ZnO injection layer. The peak position of I3$d_{5/2}$ core level shows a gradual shift from 618.9 eV in Au electrode, to 619.5 eV in perovskite and then to 620.1 eV in ZnO layer, which is probably corresponding to the bonding energy of iodide with Au, Pb and Zn metal cations in different layers, respectively[40, 41]. In contrast, XPS spectra of iodide core level in different layers of BDA-PeLEDs as shown in Supplementary Fig. 18 demonstrate that there is not any obvious iodide observed in the Au electrode, and the iodide composition in ZnO layer of BDA-PeLEDs is relatively lower than that of 3D-PeLEDs. It implies a more reliable electrochemical stability of BDA-DJ perovskite material deposited on ZnO/PEIE layer. The XPS spectra of Pb core levels shows that a new peak appears at 136.9 eV, indicating the formation of metallic Pb^0 at the interface between perovskite and ZnO as shown in Supplementary Fig. 19. With the increase of etching time to 770.9 s which represents the ion distribution in ZnO, the peak intensity of Pb^0 is further increased which confirms the penetration of Pb into underneath layer. The formation of Pb^0 can lead to a high density of deep-level trap centers, which would significantly deteriorate both the EL performance and the operational lifetime. It is noteworthy that the monatomic sputter source would moderately increase the Pb^0 concentration in the XPS results[42]. The chemical stability of BDA-DJ perovskite on ZnO surface is further confirmed by long-time storing under high temperature as shown in Supplementary Fig. 20. Therefore, the superior lifetime under large current bias for BDA-PeLEDs all comes down to the excellent electrochemical stability, which can significantly prevent the chemical reaction at the interface between perovskite and metal oxide layer, and mitigate the ion migration into the adjacent transporting layer under electric stress.

Discussion

The poor operational lifetime of PeLEDs is attributed to the electrochemical instability of perovskite emitting layer. To increase the operational lifetime under large electric field, an alkyldiammonium cation BDA^{2+} with a moderate molecular size is incorporated to form DJ perovskite phases, which can effectively enhance interlayer coupling in the 2D phase, block ion diffusion process and suppress the interfacial reaction in the PeLEDs. Through judiciously tuning the phase composition, the near-infrared 1.8FA BDA-PeLED shows a record-long operational lifetime T_{50} of 189.4 h at a high current of 100 mA cm^{-2} and 589 h at 50 mA cm^{-2}. Moreover, the device maintains its initial performance upon 10000 times of ON-OFF switching under a periodic pulse. The EQE value reaches to 16.4% after optimizing the charge transport nature of the BDA-DJ perovskite. Degradation mechanism demonstrates that the main causes

of the short lifetime in PeLEDs without BDA are the migration process of iodide anions, severe chemical reaction between perovskite and metal oxide layers under high electric field, leading to the formation of high density of Pb^0 deep-level traps and interdiffusion of Zn^{2+} and I^- ions at the interface. The record lifetime suggests that the suppressed interfacial electrochemical reaction by alkyldiammonium can provide effective solutions to the stability issue of PeLEDs.

Methods

Materials: Formamidinium iodide (FAI; ≥99%, anhydrous) was purchased from Merck. 1,4-butanediamine iodide ($BDAI_2$; 99%) was acquired from Xi'An Polymer LightTechnology Corp. Lead iodide (PbI_2; 99.999%) was procured from Tokyo Chemical Industry. Zinc acetate dehydrate ($Zn(Ac)_2{\cdot}2H_2O$) purchased from Aladdin Reagents. Tetramethyl ammoniumhydroxid pentahydrate (TMAH; 97%) was purchased from J&K scientific Ltd. Ethanolamine (99%) was purchased from Thermo Fisher Scientific Inc. Poly[(9,9-dioctylfluorenyl-2,7-diyl)-co-(4,4'-(N-(p-butylphenyl))diphenylamine) (TFB, molecular weight: 10000-200000) was acquired from American Dye Source). Polyethylenimine 80% ethoxylated solution (PEIE) was purchased from Sigma-Aldrich. All the organic solvents were procured from Sigma-Aldrich unless specifically stated.

PeLED device fabrication：The ITO substrates with size of 12×12 mm^2 were cleaned sequentially with detergent, deionized water, acetone, isopropanol and ethanol for 15 min each and then treated with ultraviolet-ozone for 30 min. The ZnO nanocrystals in ethanol solution were spin-coated onto the substrate at 5000 r.p.m. for 30 s, and then annealed in air at 150 °C for 30 min. The ZnO nanocrystals were synthesized by a simple precipitation method according to previous report[42]. After cooling down of the ZnO film, PEIE solution (4 wt% in 2-methoxyethanol) was spin-coated on ZnO surface at 5000 r.p.m. for 45 s, and then annealed in air at 90 °C for 10 min. Then the substrates were transferred to N_2 glovebox for further deposition of perovskite emitting layer and hole injection layer. 3D $FAPbI_3$ perovskite precursor was prepared by dissolving FAI and PbI_2 in *N, N*-dimethylformamide (DMF) solvent with the molar ratio of 1 or 1.8 and a concentration of 0.13 M. BDA-DJ perovskite solution with different *n* values (*n*=1-6) were prepared by dissolving $BDAI_2$, PbI_2 and FAI in DMF with the molar ratio according to the formula $BDAFA_{n-1}Pb_nI_{3n+1}$ and Pb concentration of 0.13 M. For BDA-DJ perovskite with excess FA addition, excess FAI was dissolved in DMF precursor with FA to Pb ratio ranging from 1.7 to 2.3. Perovskite precursor was spin-coated on ZnO/PEIE surface at 4000 r.p.m for 30 s and 100 mL antisolvent chlorobenzene was drop casted on the perovskite surface at 13 s during the spin coating process. Then the perovskite thin films were annealed at 100 °C for 15 min or 140 °C for 10 min to optimize the crystallization. TFB solution with a concentration of 16 mg mL^{-1} in m-xylene was spin-coated on top of perovskite surface at 3000 r.p.m. After that, the substrates were transferred to thermal evaporation chamber and 7 nm MoO_x and 60 nm Au were evaporated sequentially as the electrode under a vacuum <5×10^{-7} Torr and the emission area is 2×1.5 mm^2 as defined by shadow mask during evaporation.

Characterizations of EL performance and stability properties

The current density-voltage-radiance (*J-V-R*) performance was characterized by a Keithley 2400 source meter and a fiber optic integrating sphere coupled with a QE65 Pro spectrometer (Ocean Optics). The PeLEDs were characterized on top of the integrating sphere which collects the radiance from the bottom of the transparent ITO substrates in N_2 glovebox. The absolute radiance intensity was calibrated by a standard Vis-NIR light source (HL-3P-INT-CAL, Ocean Optics). The EL performance was recorded with the first voltage forward scan at a rate of 0.5 V s^{-1}. The operational stability of PeLEDs was conducted under a constant current density of 100 mA cm^{-2} in N_2 glovebox. EQE, radiance intensity and voltage values were tracked at the same time during the stability test.

Materials characterizations

UV-Vis absorption spectra and XRD characterizations. The UV-Vis absorption spectra were measured by a Hitachi U-3501 UV-visible-NIR spectrophotometer. The XRD patterns of the thin films were carried out by a Rigaku SmartLab X-ray diffractometer equipped with Cu K_a (l=1.54 Å) and a HyPix-3000 2D hybrid pixel array detector.

GIWAXs characterizations: The GIWAXS were conducted at 23 A SWAXS beamline, using a 10 keV primary beam, 0.1° incident angle, Pilatus 1M-F and C9728 detector.

SEM and TEM characterizations: SEM images were obtained using a FEI Quanta 400 field emission scanning electron microscope (FESEM, FEI) with an accelerating voltage of 10 kV. The TEM images were captured by a field emission transmission electron microscopy (FEI TecnaiF20) at 200 kV.

Steady-state PL characterizations: PL spectra were measured by commercially available Raman/PL spectrometer (Horica, Inc.) with an air-cooled double frequency Nd: Yag 532 nm laser source and a power of 70 mW cm^{-2}.

XPS characterizations: The ion depth profile was performed by XPS surface analysis system (Thermo Fisher Scientific, ESCALAB 250) equipped with Al K_a X-ray gun (*hn*=1486.6 eV) for etching purpose. The diameter of the etching area is 200 μm and Ar^+ sputter source was operated at 2 KeV.

TRPL characterizations: For the TRPL characterizations, a frequency doubled (400 nm) 100 fs Ti: sapphire oscillator operating at a 200 KHz rate was focused to a spot of ~100 μm to excite the encapsulated perovskite films. PL was collimated and focused onto the monochromator (Acton Spectrapro 275) slit. The PL was dispersed onto a single photon detector to carry out the measurements.

TA spectroscopy: The transient dynamics in fs-ns time region (50 fs - 7 ns) was acquired by Helios that works in a nondegenerate pump–probe configuration. The pump pulses were generated from an optical parametric amplifier (OPerA Solo) that was pumped by a 1 kHz regenerative amplifier (Coherent Legend, 800 nm, 150 fs, 4 mJ). A mode lock Ti-sapphire oscillator (Coherent Vitesse, 100 fs, 80 MHz) was used to seed the amplifier. A beta barium borate (BBO) crystal was used to double the frequency of 800 nm for

pump at 400 nm. The probe pulse was a white light continuum and generated by passing the 800 nm fs pulses through a 2 mm sapphire plate for visible part (420-780 nm).

Declarations

Data availability.

The data that support the plots within this paper and other finding of this study are available from the corresponding author upon request.

Acknowledgements

The work is in part supported by ITS/088/17, ITS/390/18 by Innovation and Technology Commission, Hong Kong SAR Government, Science and Technology Program of Guangzhou (No. 2019050001), Research Grants Council of Hong Kong, particularly, via Grant Nos. AoE/P-03/08, T23-407/13-N,AoE/P-02/12, 14204616, 14203018, N_CUHK438/18, and CUHK Group Research Scheme, the Natural Science Foundation of Guangdong Province (No. 2019B151502028), and CUHK Postdoctoral Fellowship.

Author contributions

M. Z. Long and J. B. Xu conceived the idea and designed the experiments as well as supervised the work. K. H. Ngai and M. Z. Long conducted the materials syntheses and device fabrication. Q. Wei and G. C. Xing performed the TA characterizations and analyzed the results. C. C. S. Chan and K. S. Wong conducted the TRPL results and analyzed the results. Z. F. Chen, K. H. Ngai and X. L. Guo performed electrical and optical properties measurements. M. C. Qin and X. H. Lu performed the GIWAXS measurement and analysis. F. Y. Xie performed the XPS characterization. All authors discussed the results and prepared the manuscript. M. Z. Long and J. B. Xu supervised the whole project. All authors discussed the results and contributed to the writing of the paper.

Additional information

Supplementary information is available in the online version of the paper. Reprints and permissions information is available online at www.nature.com/reprints. Correspondence and requests for materials should be addressed to M. Z. Long and J. B. Xu.

Competing financial interests

The authors declare no competing financial interests.

References

1. Tan Z. -K., *et al*. Bright light-emitting diodes based on organometal halide perovskite. *Nat. Nanotechnol.* **9**, 687-692 (2014).

2.Cho H., *et al*. Overcoming the electroluminescence efficiency limitations of perovskite light-emitting diodes. *Science* **350**, 1222-1225 (2015).

3. Wang N. N., *et al*. Perovskite light-emitting diodes based on solution-processed self-organized multiple quantum wells. *Nat. Photonics* **10**, 699-704 (2016).

4. Lin K. B., *et al*, Perovskite light-emitting diodes with external quantum efficiency exceeding 20 percent. *Nature* **562**, 245-248 (2018).

5. Cao Y., *et al*., Perovskite light-emitting diodes based on spontaneously formed submicrometre-scale structures. *Nature* **562**, 249-253 (2018).

6. Xu W. D., *et al*., Rational molecular passivation for high-performance perovskite light-emitting diodes. *Nat. Photonics* **13**, 418-424 (2019).

7. Liu Y., *et al*., Efficient blue light-emitting diodes based on quantum-confined bromide perovskite nanostructures. *Nat. Photonics* **13**, 760-764 (2019).

8. Song J. Z., *et al*., Quantum dot light-emitting diodes based on inorganic perovskite cesium lead halides ($CsPbX_3$). *Adv. Mater.* **27**, 7162-7167 (2015).

9. Bade S. G. R., *et al*., Fully printed halide perovskite light-emitting diodes with silver nanowire electrodes. *ACS nano* **10**, 1795-1801 (2016).

10. Jeong S.-H., *et al*., Universal high work function flexible anode for simplified ITO-free organic and perovskite light-emitting diodes with ultra-high efficiency. *NPG Asia Mater.* **9**, e411 (2017).

11. Zhao B. D., *et al*., High-efficiency perovskite–polymer bulk heterostructure light-emitting diodes. *Nat. Photonics* **12**, 783-789 (2018).

12. Chiba T., *et al*., Anion-exchange red perovskite quantum dots with ammonium iodine salts for highly efficient light-emitting devices. *Nat. Photonics* **12**, 681-687 (2018).

13. Cho H., *et al*., Improving the stability of metal halide perovskite materials and light-emitting diodes. *Adv. Mater.* **30**, 1704587 (2018).

14. Li N., *et al*., Stabilizing perovskite light-emitting diodes by incorporation of binary alkali cations. *Adv. Mater.* **32**, 1907786 (2020).

15. Zhao L. F., *et al*., Thermal Management Enables Bright and Stable Perovskite Light-Emitting Diodes. *Adv. Mater.*, **32**, 2000752 (2020).

16. Zhao L. F., *et al*., Improved Outcoupling Efficiency and stability of perovskite light-emitting diodes using thin emitting layers. *Adv. Mater.* **31**, 1805836 (2019).

17. Xing J., *et al.*, Color-stable highly luminescent sky-blue perovskite light-emitting diodes. *Nat. Commun.* **9**, 1-8 (2018).

18. Prakasam V., *et al.*, Degradation mechanisms in organic lead halide perovskite light-emitting diodes. *Adv. Optical Mater.* **7**, 1900902 (2019).

19. Lee S., *et al.*, Amine-based passivating materials for enhanced optical properties and performance of organic–inorganic perovskites in light-emitting diodes. *J. Phys. Chem. Lett.* **8**, 1784-1792 (2017).

20. Dong Q., *et al.*, Operational stability of perovskite light emitting diodes. *J. Phys. Mater.* **3**, 012002 (2020).

21. Oranskaia A., *et al.*, Halogen Migration in Hybrid Perovskites: The Organic Cation Matters. *J. Phys. Chem. Lett.* **9**, 5474-5480 (2018).

22. Zhumekenov A. A., *et al.*, Formamidinium lead halide perovskite crystals with unprecedented long carrier dynamics and diffusion length. *ACS Energy Lett.* **1**, 32-37 (2016).

23. Yang M., *et al.*, Reduced efficiency roll-off and enhanced stability in perovskite light-emitting diodes with multiple quantum wells. *J. Phys. Chem. Lett.* **9**, 2038-2042 (2018).

24. Yuan M. J., *et al.*, Perovskite energy funnels for efficient light-emitting diodes. *Nat. Nanotechnol.* **11,** 872–877 (2016).

25. Byun J. W., *et al.*, Efficient visible quasi-2D perovskite light-emitting diodes. *Adv. Mater.* **28**, 7515–7520 (2016).

26. Kim H., *et al.*, Proton-transfer-induced 3D/2D hybrid perovskites suppress ion migration and reduce luminance overshoot, *Nat. Commun*. **11**, 3378 (2020)

27. Cheng T., *et al.*, Ion Migration-Induced Degradation and Efficiency Roll-off in Quasi-2D Perovskite Light-emitting Diodes. *ACS Appl. Mater. Interfaces*, **12**, 33004–33013, (2020).

28. Miao Y. F., *et al.*, Stable and bright formamidinium-based perovskite light-emitting diodes with high energy conversion efficiency. *Nat. Commun.* **10**, 1-7 (2019).

29. Shang Y. Q., *et al.*, Highly stable hybrid perovskite light-emitting diodes based on Dion-Jacobson structure. *Sci. Adv.* **5**, eaaw8072 (2019).

30. Safdari M., *et al.*, Impact of synthetic routes on the structural and physical properties of butyl-1, 4-diammonium lead iodide semiconductors. *J. Mater. Chem. A,* **5**, 11730-11738 (2017).

31. Zhang T. Y., *et al.*, Interfacial crosslinked quasi-2D perovskite with boosted carrier transport and enhanced stability. *J. Phys. D Appl. Phys.* **51**, 404001 (2018).

32. Wang H., *et al.*, Interlayer cross-linked 2D perovskite solar cell with uniform phase distribution and increased exciton coupling. *Solar RRL* **4**, 1900578 (2020).

33. Yuan Z. C., *et al.*, Unveiling the synergistic effect of precursor stoichiometry and interfacial reactions for perovskite light-emitting diodes. *Nat. Commun.* **10**, 1-9 (2019).

34. Zou W., *et al.*, Minimising efficiency roll-off in high-brightness perovskite light-emitting diodes. *Nat. Commun.* **9**, 1-7 (2018).

35. Wang H. Y., *et al.*, Perovskite-molecule composite thin films for efficient and stable light-emitting diodes, *Nat. Commun*. **11**, 891 (2020).

36. Zhao X. F., *et al.*, Large-area near-infrared perovskite light-emitting diodes, *Nat. Photon*ics **14**, 215–218 (2020).

35. Zhao L. F., *et al.*, Electrical stress influences the efficiency of $CH_3NH_3PbI_3$ perovskite light emitting devices. *Adv. Mater.* **29**, 1605317 (2017).

36. Han T. H., *et al.*, Surface-2D/bulk-3D heterophased perovskite nanograins for long-term-stable light-emitting diodes. *Adv. Mater.* **32**, 1905674 (2020).

37. Lin Y., *et al.*, Suppressed ion migration in low-dimensional perovskites. *ACS Energy Lett.* **2**, 1571-1572 (2017).

38. Mahmoudi T., *et al.*, Stability enhancement in perovskite solar cells with perovskite/silver–graphene composites in the active layer. *ACS Energy Lett.* **4**, 235-241 (2018).

39. XPS Reference Page. http://www.xpsfitting.com/2014/03/iodine.html.

40. Long M. Z., *et al.*, Abnormal synergetic effect of organic and halide ions on the stability and optoelectronic properties of a mixed perovskite via in situ characterizations. *Adv. Mater.* **30**, 1801562 (2018).

41. Wang J. P., *et al.*, Interfacial control toward efficient and low-voltage perovskite light-emitting diodes. *Adv. Mater.* **27**, 2311-2316 (2015).

Figures

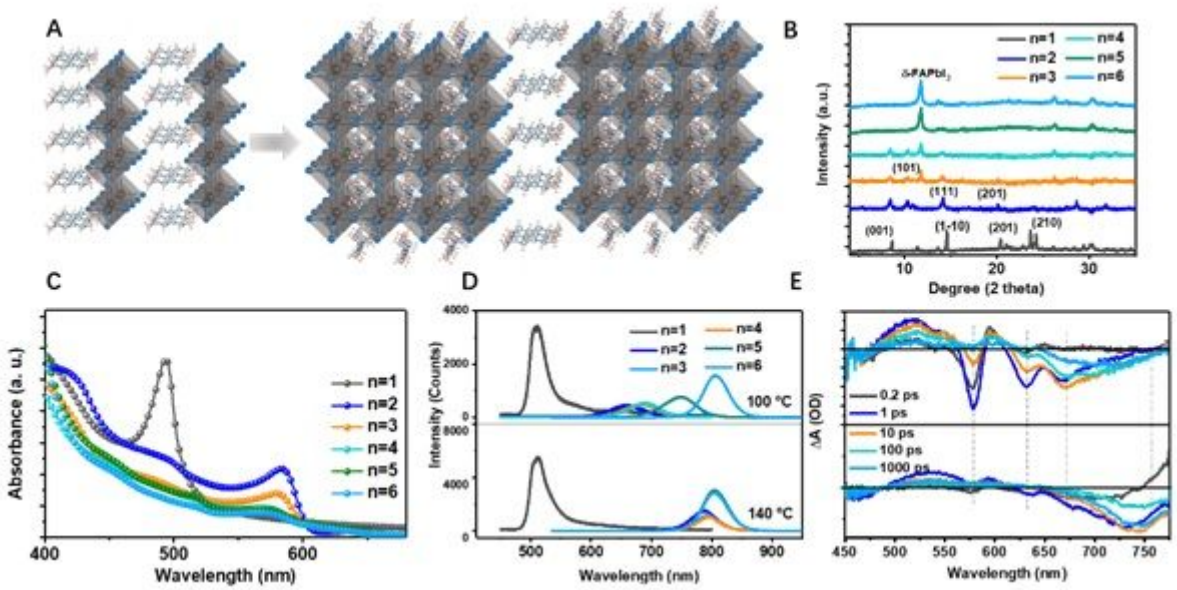

Figure 1

Characterizations of BDA-DJ thin films. (A) Schematic configuration of BDA-DJ phases with inorganic layers n=1 and 4. (B) XRD patterns of BDA-DJ perovskite with n=1-6. (C) Steady-state UV-Vis absorption spectra. (D) Steady-state PL spectra of the films after annealed at 100 °C and 140°C, respectively. (E) TA spectra of n=5 BDA-DJ thin film after annealing at 100 °C (the top) and 140°C (the bottom).

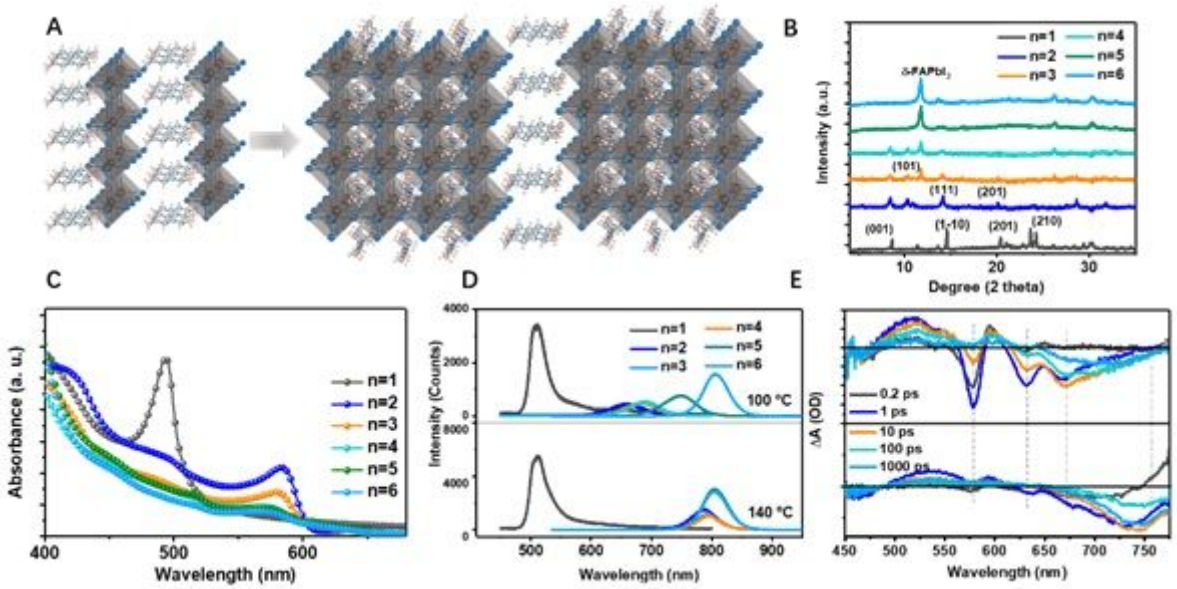

Figure 1

Characterizations of BDA-DJ thin films. (A) Schematic configuration of BDA-DJ phases with inorganic layers n=1 and 4. (B) XRD patterns of BDA-DJ perovskite with n=1-6. (C) Steady-state UV-Vis absorption spectra. (D) Steady-state PL spectra of the films after annealed at 100 °C and 140°C, respectively. (E) TA spectra of n=5 BDA-DJ thin film after annealing at 100 °C (the top) and 140°C (the bottom).

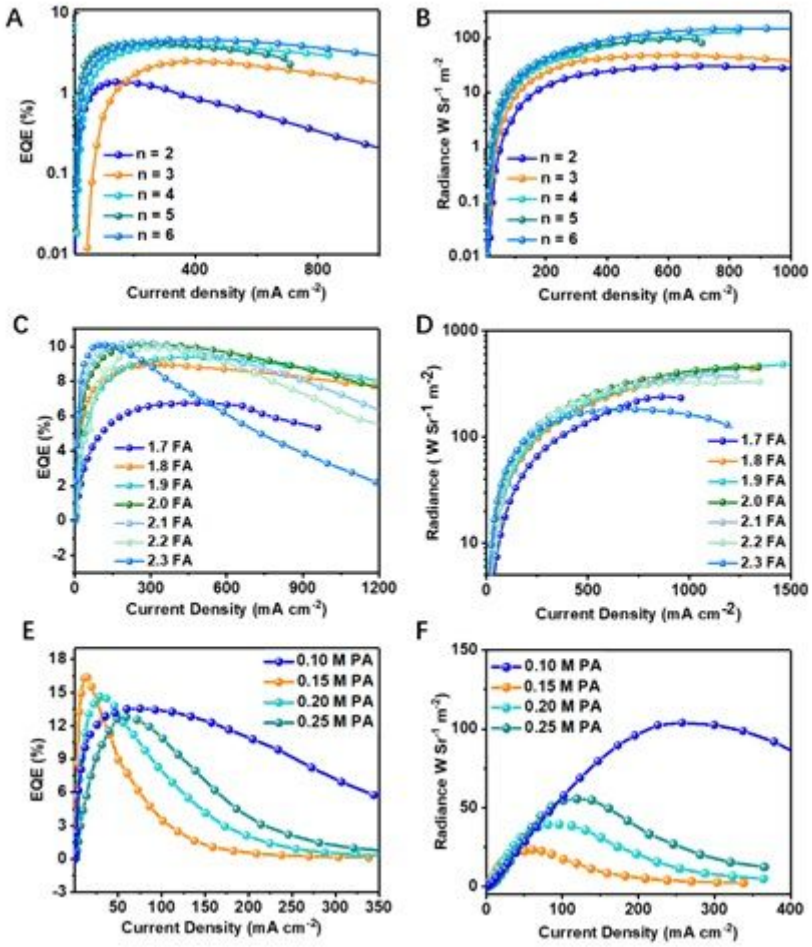

Figure 2

Electroluminescent performance of BDA-PeLEDs. (A) EQE-current density curves and (B) the corresponding radiance-current density curves of BDA-PeLEDs with different n values (n=2-6). (C) EQE-current density and (D) radiance-current density curves of n=5 BDA-PeLEDs with excess FAI addition in perovskite layer (molar ratio of FAI to PbI2 ranging from 1.7 to 2.3). (E) EQE-current density and (F) the corresponding radiance-current density curves of 1.8FA BDA-PeLEDs with the addition of different amounts of PA.

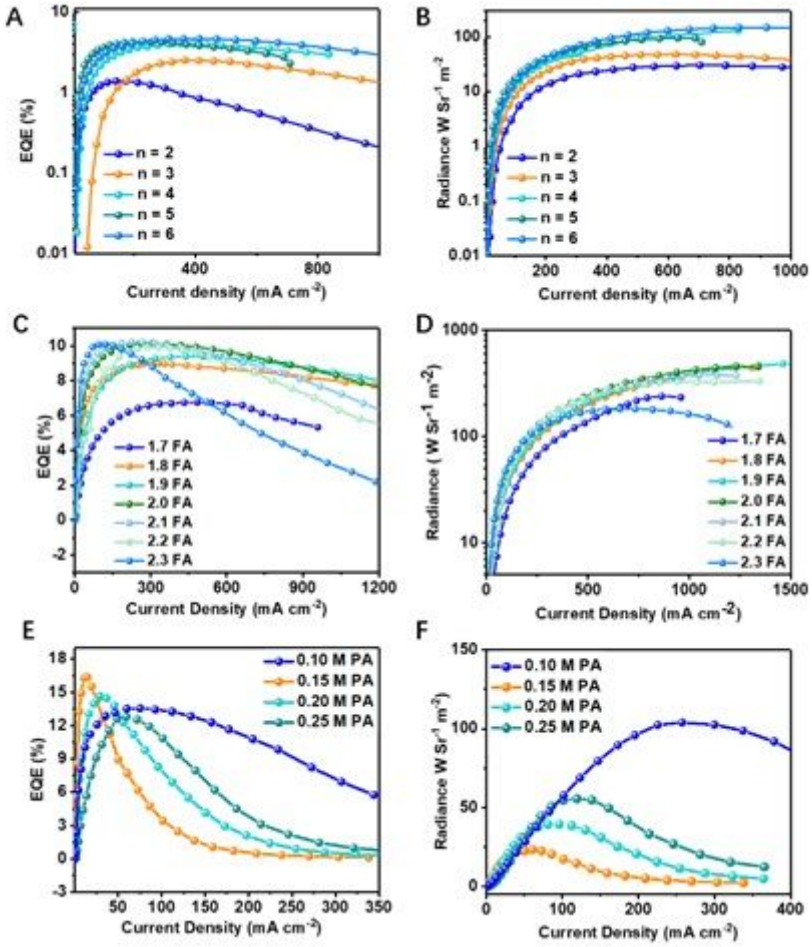

Figure 2

Electroluminescent performance of BDA-PeLEDs. (A) EQE-current density curves and (B) the corresponding radiance-current density curves of BDA-PeLEDs with different n values (n=2-6). (C) EQE-current density and (D) radiance-current density curves of n=5 BDA-PeLEDs with excess FAI addition in perovskite layer (molar ratio of FAI to PbI2 ranging from 1.7 to 2.3). (E) EQE-current density and (F) the corresponding radiance-current density curves of 1.8FA BDA-PeLEDs with the addition of different amounts of PA.

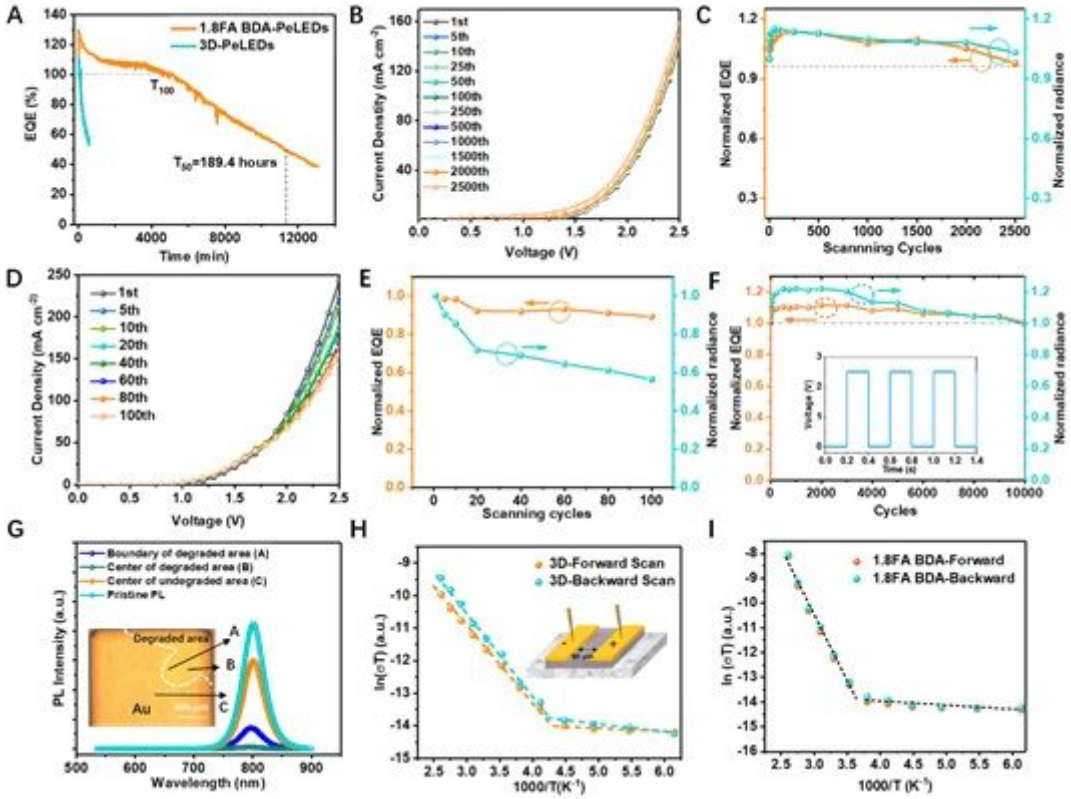

Figure 3

Operational lifetime evaluation. (A) Operational lifetime measurement for 1.8FA BDA- and 3D-PeLED under a constant current density of 100 mA cm2 and initial radiance is approximately equal to 50 W Sr1 m2 for 1.8FA BDA-PeLED. (B) Current-voltage curves of 2500 scanning cycles with scan rate of 0.5 V s1 for 1.8FA BDA-PeLEDs. (C) EQE and radiance tendency as a function of scanning cycle for 1.8FA BDA-PeLEDs. (D) Current-voltage curves of 100 scanning cycles for 3D-PeLED. (E) EQE-radiance tendency as a function of scanning cycle for 3D-PeLEDs. (F) EQE and radiance values during 10000 times of ON and OFF switching for the 1.8FA BDA-PeLEDs under a periodic pulse. The pulse voltage is 2.5 V and the periodicity is 0.4 s (2.5 Hz) as shown in the inset. (G) PL spectra of the degraded and undegraded area for 3D-PeLEDs after operation. The degraded area is marked by dash line in the inset figure. The relation between temperature (1000/T) and conductivity (ln(T)) derived from conductivity measurement with temperature ranging from 183 K to 383 K for (H) 3D and (I) 1.8FA BDA-perovskite materials. The lateral conductivity measurement configuration is displayed as the inset image.

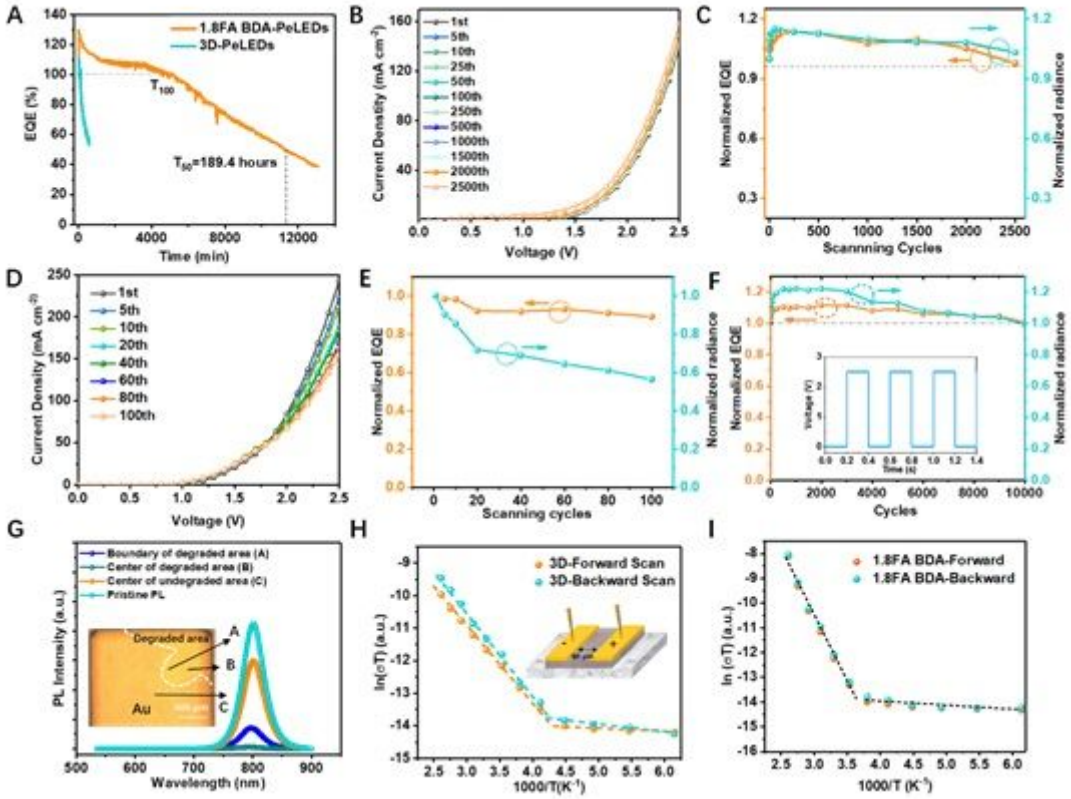

Figure 3

Operational lifetime evaluation. (A) Operational lifetime measurement for 1.8FA BDA- and 3D-PeLED under a constant current density of 100 mA cm2 and initial radiance is approximately equal to 50 W Sr1 m2 for 1.8FA BDA-PeLED. (B) Current-voltage curves of 2500 scanning cycles with scan rate of 0.5 V s1 for 1.8FA BDA-PeLEDs. (C) EQE and radiance tendency as a function of scanning cycle for 1.8FA BDA-PeLEDs. (D) Current-voltage curves of 100 scanning cycles for 3D-PeLED. (E) EQE-radiance tendency as a function of scanning cycle for 3D-PeLEDs. (F) EQE and radiance values during 10000 times of ON and OFF switching for the 1.8FA BDA-PeLEDs under a periodic pulse. The pulse voltage is 2.5 V and the periodicity is 0.4 s (2.5 Hz) as shown in the inset. (G) PL spectra of the degraded and undegraded area for 3D-PeLEDs after operation. The degraded area is marked by dash line in the inset figure. The relation between temperature (1000/T) and conductivity (ln(T)) derived from conductivity measurement with temperature ranging from 183 K to 383 K for (H) 3D and (I) 1.8FA BDA-perovskite materials. The lateral conductivity measurement configuration is displayed as the inset image.

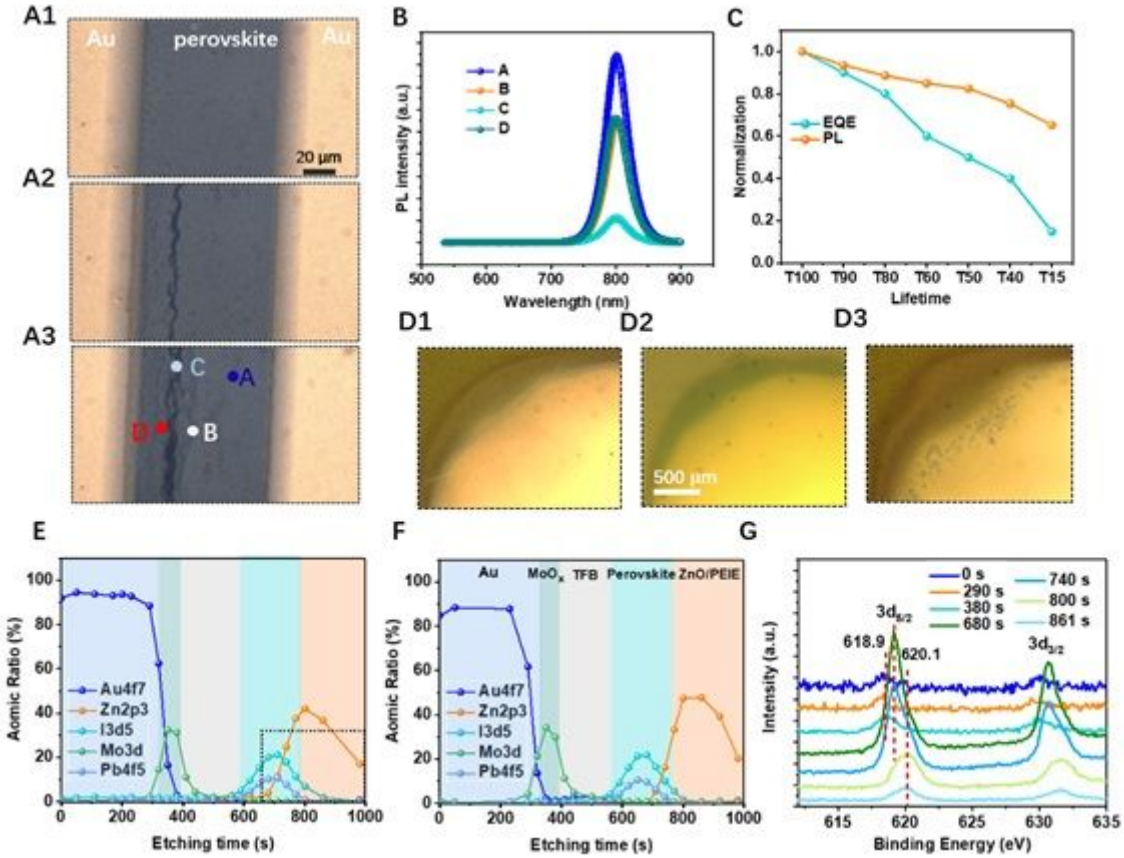

Figure 4

Degradation behavior of PeLEDs. (A) In-situ observation of the degradation process of 3D FAPbI3 perovskite film under a constant lateral electric field. The lateral channel length is 80 μm and electric field is 0.44 V μm1 at 35 V. The A1, A2 and A3 figures present the perovskite films with biasing time of 0, 15 min and 30 min, respectively. (B) PL spectra of different spots in the degraded perovskite thin film as marked in Fig. 4A3. (C) The variation tendency of EQE value and PL intensity for 3D-PeLED at degradation stages of Tx (x=90, 80, 60, 50, 40 and 15), where Tx is the time required for EQE dropping to x% of its initial value. (D) The optical images of gold electrode of 3D-PeLEDs at degradation stages of T100 (D1), T50 (D2) and T20 (D3), respectively. (E, F) XPS depth profile analyses of vertical ion distribution including Au4f, Zn2p, Mo3d, Pb4f and I3d (C1s and O1s are not displayed here) in 3D-PeLED and 1.8FA BDA-PeLED after operating at 100 mA cm2 for 20 h. (G) XPS spectra of I3d core level at etching time of 0 s and 290.3 s, 380.6 s, 680.8 s and 740.8 s, 800.9 s and 861.0 s, which represent the distribution of iodine species in Au electrode, TFB organic layer, perovskite layer and ZnO layer in 3D-PeLEDs, respectively.

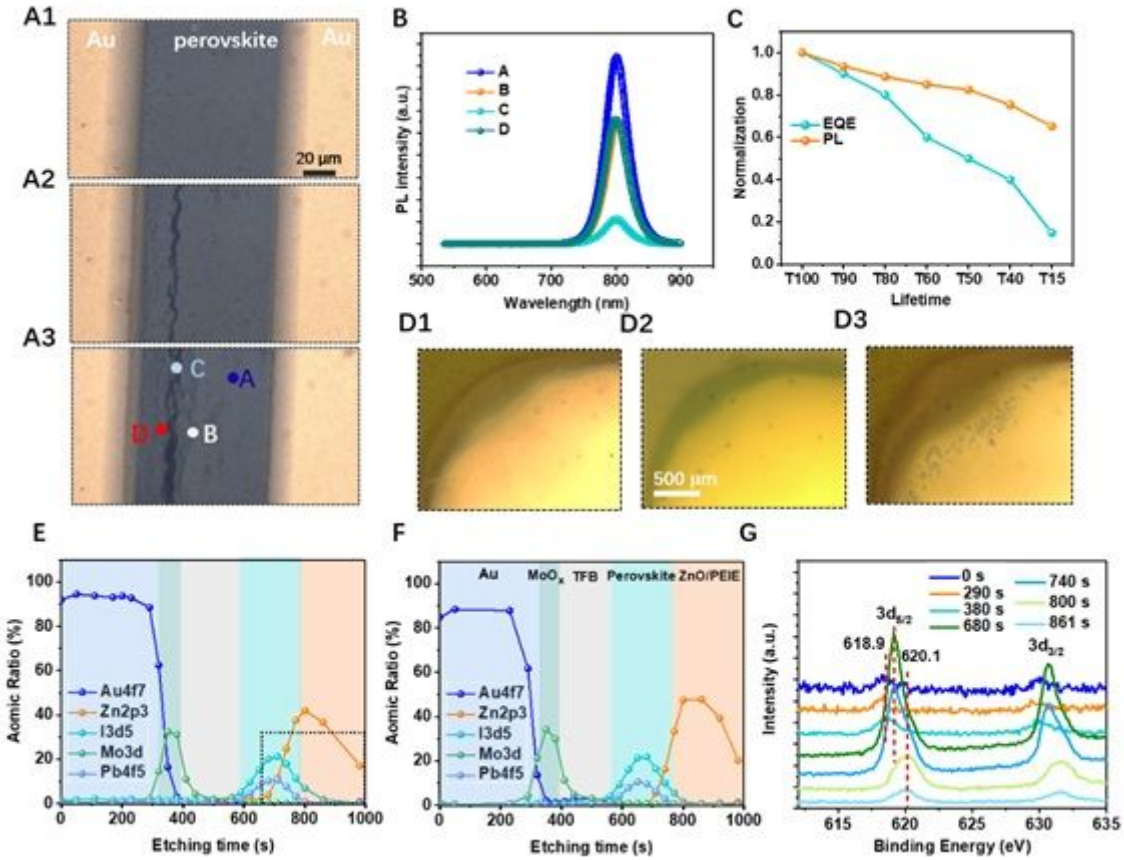

Figure 4

Degradation behavior of PeLEDs. (A) In-situ observation of the degradation process of 3D FAPbI3 perovskite film under a constant lateral electric field. The lateral channel length is 80 μm and electric field is 0.44 V μm1 at 35 V. The A1, A2 and A3 figures present the perovskite films with biasing time of 0, 15 min and 30 min, respectively. (B) PL spectra of different spots in the degraded perovskite thin film as marked in Fig. 4A3. (C) The variation tendency of EQE value and PL intensity for 3D-PeLED at degradation stages of Tx (x=90, 80, 60, 50, 40 and 15), where Tx is the time required for EQE dropping to x% of its initial value. (D) The optical images of gold electrode of 3D-PeLEDs at degradation stages of T100 (D1), T50 (D2) and T20 (D3), respectively. (E, F) XPS depth profile analyses of vertical ion distribution including Au4f, Zn2p, Mo3d, Pb4f and I3d (C1s and O1s are not displayed here) in 3D-PeLED and 1.8FA BDA-PeLED after operating at 100 mA cm2 for 20 h. (G) XPS spectra of I3d core level at etching time of 0 s and 290.3 s, 380.6 s, 680.8 s and 740.8 s, 800.9 s and 861.0 s, which represent the distribution of iodine species in Au electrode, TFB organic layer, perovskite layer and ZnO layer in 3D-PeLEDs, respectively.

Supplementary Files

This is a list of supplementary files associated with this preprint. Click to download.

- SupplementeryInformationNatCommun.docx

- SupplementeryInformationNatCommun.docx